Metal-to-insulator transition and superconductivity in boron-doped diamond

Etienne Bustarret, Philipp Achatz, Benjamin Sacépé, Claude Chapelier, Christophe Marcenat, Luc Ortega, Thierry Klein

Metal-to-insulator transition and superconductivity in boron-doped diamond

E. Bustarret[1], P. Achatz[1,2], B. Sacépé[2], C. Chapelier[2], C. Marcenat[2], L. Ortéga[1] and T. Klein[1,3]

[1)] Institut Néel, CNRS, 25 av. des Martyrs, 38042 Grenoble, France
[2)] CEA-Grenoble, DRFMC, 38054 Grenoble, France
[3)] Université Joseph Fourier, Boite Postale 53, 38041 Grenoble, France

Corresponding author :
etienne.bustarret@grenoble.cnrs.fr
Phone : +33 476 88 74 68 Fax : +33 476 88 79 88

The experimental discovery of superconductivity in boron-doped diamond came as a major surprise both to the diamond and to the superconducting materials communities. The main experimental results obtained since then on single-crystal diamond epilayers are reviewed and confronted to calculations, and some open questions are identified. The critical doping of the metal-to-insulator transition (MIT) was found to coincide with that necessary for superconductivity to occur. Some of the critical exponents of the MIT were determined and superconducting diamond was found to follow a conventional type II behaviour in the dirty limit, with relatively high critical temperature values quite close to the doping-induced insulator-to-metal transition. This could indicate that on the metallic side, both the electron-phonon coupling and the screening parameter depend on the boron concentration. To our view, doped diamond is a potential model-system for the study of electronic phase transitions and a stimulating example for other semiconductors such as germanium and silicon.

Keywords : Diamond, boron-doping, superconductivity, metal-insulator transition

Introduction

In 2004, bridging the gap separating the superhardness and the superconducting communities, Ekimov et al [1] discovered the superconducting behaviour of a diamond sample resulting from annealing graphite with B_4C at 2500-2800 K under 8-9 GPa for 5s. These authors proposed also a mechanism for the transformation of graphite into diamond at high pressure and high temperature (HPHT), and made a thorough characterization of the diamond polycrystal [2]. Similar results were reported shortly after for polycrystalline [3,4] and (100)-oriented single crystal [5] diamond films grown by microwave plasma-assisted chemical vapour deposition (MPCVD), showing that "zero" resistivity could be observed up to the boiling temperature of helium (4.2 K), that doping-induced superconductivity appeared above about 6 10^{20} B/cm^3 and that T_c increased with the Boron concentration.
Other methods such as chemical transport reaction [6] and hot filament-assisted [7] chemical vapour deposition, as well as heavily boron-doped nanocrystalline diamond deposited on seeded glass substrates [8], were also shown to yield superconducting layers under appropriate conditions, confirming the robustness of Ekimov's seminal observation. Up to now, T_c has been found to reach the 8-10 K range in a few cases [4,7,9], the exact values depending not only on the preparation method and conditions but also on the experimental characterisation and data analysis procedures applied to the transition.

A few years before that, the stunning success of graphite-like MgB_2, with a superconducting transition temperature T_c of 39 K [10], and the striking properties of many graphite intercalation compounds had shown such light atom-based layered structures to be favourable to superconductivity, as for example in CaC_6 where T_c reaches 11.5 K [11]. Shortly after Ekimov's discovery, calculations of the band structure of B-doped diamond [12-16], combined with the assumption of a BCS-type pairing mechanism [17], suggested that superconductivity arose from the coupling (V_c potential) of phonons with holes at the top of the σ bonding (valence) bands, in a way similar to MgB_2. However, the 3D nature of the sp^3-hybridized carbon network in diamond leads to a density of states at the Fermi level g_F much weaker than in the quasi-2D MgB_2 compound where B is sp^2 hybridized. This results in a lower (calculated) coupling constant $\lambda = g_F V_c$ on the order of 0.4 in diamond doped with 5% holes instead of up to 1 in MgB_2.
The possibility for a superconducting state to arise in a degenerate semiconductor or a semimetal has been theoretically explored in the late 1950's and early 1960's [18-19]. Experimentally, after many unsuccessful attempts, type II superconducting transitions were observed between 50 mK and 500 mK in self-doped GeTe, SnTe and reduced $SrTiO_3$. In all three cases, $H_c(T_c)$ phase diagrams were obtained, while specific heat measurements established the bulk character of the transition. Finally, tunnel spectroscopy performed on GeTe [20], measured the superconducting gap width 2Δ and showed that a $2\Delta/k_BT_c$ ratio of 4.3 could be estimated. These results were considered at the time to further validate the BCS model [17] for superconductivity [19]. Despite this apparent success, the "superconducting semiconductors" angle had not raised much interest during several decades, until Ekimov's results [1] triggered a renewed excitement, which will probably last for some time, now that superconductivity has been also induced by heavy boron doping in the parent silicon crystal [21]. We shall stress here the features specific to diamond that could lead this crystal to become a model-system for this class of materials.

Boron incorporation at high concentrations

In diamond, contrary to nitrogen, boron is readily incorporated on substitutional bonding sites of the lattice, and behaves as an electronic acceptor centre with an ionisation energy of about 370 meV. In the 10^{20}-10^{21} cm^{-3} boron concentration range of interest here, polycrystalline p^{++} films grown by MPCVD on Si substrates as well as nanocrystalline layers (which have industrial applications as chemically inert electrodes for advanced electrochemical sensing or processing devices) have been found to have electrical properties similar (at room temperature) to those of their single crystal counterparts. We shall therefore focus here mostly on single crystal epilayers grown by MPCVD which are generally better suited for quantitative studies.
As a result of the larger covalent radius of boron (r_B = 0.88Å) compared to that of carbon (r_C = 0.77 Å), the substitutional introduction of boron into diamond leads to an expansion of the lattice parameter. This has been found to follow the linear interpolation attributed to Vegard as long as the boron content was lower than 0.2 at.% in MPCVD epilayers [22, 23]. Above those threshold concentrations, the expansion is less pronounced [23,24]. This lower expansion rate has been attributed both to the contribution of free holes [23], to the negative deformation potentials at the valence band maximum [22] and to the occurrence of substitutional boron pairs [24] which are stabilized by p-type doping [25]. In homoepitaxial films, this expansion is severely limited in the film plane by pseudomorphic growth under compressive biaxial stress, but the boron-induced positive strain along the growth direction is easily detected in the double crystal X-ray diffraction curves [26]. A typical data set obtained at room-temperature on both a (100)- oriented and a (111)-oriented homoepitaxial film is represented by intensity contours in figs. 1a and 1b and shows that the down-shifted {400}

and {111} diffraction peaks originating from the epilayer have a lineshape very similar to that of the type Ib diamond substrate. In particular, the width of the rocking curve along the vertical axis (omega-scan) shows that the mosaicity of the HPHT substrate is maintained in the epilayer for both orientations, whereas the strain distribution represented by the lineshape along the horizontal axis (2 theta - omega scan) became somewhat broader in the epilayer.
Finally, the possibility of non-substitutional boron incorporation at high doping levels has been investigated by photoelectron intensity angular distribution circular dichroism [27] and by Nuclear Magnetic Resonance (NMR) on the ^{11}B isotope [9]. Both studies confirmed that the main incorporation site for boron was substitutional. However, ^{11}B-NMR studies detected a second boron bonding site of lower symmetry, most abundant in relatively thin (100)-oriented epilayers, and which was proposed to be a local B-H complex [9]. Hydrogen is known to be present in MPCVD diamond layers and to passivate effectively boron acceptors as well as other defects [28]. Interstitial boron as well as boron-vacancy or boron-self-interstitial pairs are also mentioned in the literature but the stability of these incorporation sites has been questioned.

Doping-induced Metal-to-Insulator transition (MIT)
As seen in fig. 2, when the boron concentration, n_B, was increased from 4 to about 5 10^{20} cm^{-3}, the low-temperature transport properties of (100)-oriented p^{++} layers changed drastically from an insulating behaviour (i.e. the resistivity diverges when $T \rightarrow 0$) to a metallic (and even superconducting) T-dependence which extrapolated to a finite normal-state resistivity value at zero temperature. Given the 10% uncertainty of SIMS absolute calibrations, these experimental results are in excellent agreement with the zero temperature model calculations of the vanishing ionization energy or of the chemical potential for both the insulating and the metallic phase [26], which yield a critical boron concentration n_c around 5.2 10^{20} cm^{-3}. A generalized Drude approach, taking into account the influence of temperature but neither the hopping transport nor weak localization effects, has also been applied to this system [29] and yielded a similar critical concentration value lying between 4 and 5 10^{20} cm^{-3}.
Following Mott, we may assume that this transition results from boron-related hydrogenic states with a Bohr radius $a_H = \varepsilon a_0/m^*$ which overlap when n_B reaches n_c with $a_H n_c^{1/3} = 0.26$ as observed in numerous materials. In this case, taking $\varepsilon = 5.7$ for diamond and $m^* = 0.74$ for the holes, the Bohr radius a_H is estimated at 0.35 nm in fair agreement with values based on the acceptor excited states. The present experimental and theoretical estimates for n_c agree with experimental data recently obtained on free standing polycrystalline p^{++} layers where $n_c < 4.5\ 10^{20}$ cm^{-3} [30] and $3.4\ 10^{20}$ $cm^{-3} < n_c < 5.5\ 10^{20}$ cm^{-3} [4]. However, they are one order of magnitude lower than those measured in ion-implanted diamond [31] where the doping efficiency may be strongly reduced by the non-substitutional incorporation of boron discussed above.
Below the critical boron concentration, the resistivity increases as $\rho = \rho_0 \exp(T_0/T)^m$, where the value of the exponent m depends on the hopping mechanism : m = 1 for hopping to the nearest accessible site, m = ¼ for variable range hopping (VRH) assuming [32] a nearly constant density of states at the Fermi level g_F, and m = ½ when g_F is reduced by a Coulomb gap (ES regime [33]). The T_0 parameter is related to the localisation length ξ_{loc} which is of the order of the Bohr radius far from the metal-non metal transition, in a concentration range where the formation of both the impurity band and the valence band tail are expected. Typical values of 10^6 K and crossovers from the VRH to the ES regime and then to a m=1 variation at even lower temperature have been reported for type IIb single crystals with $n_B = 2\ 10^{19}$ cm^{-3} [34]. Closer to the transition, ξ_{loc} is expected to increase, leading to lower T_0 values, so that the VRH regime extends to lower temperatures, as is the case in fig. 2 where T_0 is on the

order of a few 10^3 K for n_B = 2.4 10^{20} cm^{-3} and several 10^2 for n_B = 4 10^{20} cm^{-3} with a VRH regime extending down to 10 K [29].

Above the critical concentration, the normal state conductivity can be extrapolated to a finite value σ_0 as $T \rightarrow 0$ K, as deduced from the resistivity variations shown in fig. 2. As a matter of fact, as shown in the inset of fig. 3a, for n_B greater than 6 10^{20} cm^{-3} [29], and below a certain temperature at which the inelastic mean free path becomes of the order of the elastic one, the resistivity increases slowly when the temperature is reduced. In this regime, where weak localisation effects arising from electron-phonon scattering are expected as well as other electronic correlations, the experimental temperature dependence of the conductivity was found [29] to follow between 3 and 30 K an expression of the type : $\sigma = \sigma_0 + AT^{1/2} + B_{e\text{-}ph}T$. Pronounced "weak localisation" effects have been detected also in heavily boron-doped polycrystalline [4] and nanocrystalline [35] diamond, while a $\sigma = \sigma_0 + AT^{1/3}$ variation has been observed in ion-implanted samples [31].

The critical regime of a second order phase transition is generally described by two characteristic exponents, ν and η [36]. ν relates the correlation length (here ξ_{loc}) to the external parameter driving the transition (here n_B) through $\xi_{loc} \sim 1/|n_B\text{-}n_c|^{\nu}$, whereas η relates the energy and length scales of the system ($E \sim 1/L^{\eta}$). It has been suggested [36] that η ranges from 1 to 3 depending on the relative importance of one electron localisation, many body correlations and screening effects, and there are some preliminary indications [4,29] that for p^{++} diamond $\eta \approx 3$ in agreement with the results obtained on doped silicon. As σ is expected to vary as $1/\xi_{loc}$, one expects [36] that $\sigma_0 = 0.1(e^2/\hbar)/\xi_{loc}$ with $a_H/\xi_{loc} = (n_B/n_c - 1)^{\nu}$. As shown in fig. 3a (solid line), σ_0 follows closely the prediction of the scaling theory with $\nu = 1$ and without any other adjustable parameter [29]. In contrast to η, a unique ν value on the order of 1 has been obtained numerically in all systems, independent of the relative importance of the one electron and many-body effects. The $\nu = 1.7$ value reported previously [31] for implanted diamond remains thus to be explained.

Doping-induced Normal-to-Superconducting transition

Although an increase of T_c with either the boron concentration n_B or the free carrier density has been expected on the basis of VCA calculations [14-16,37] and experimentally observed in some of the early reports [4, 5, 26], systematic studies have remained rather scarce. Assuming that the mechanism for superconductivity was that proposed by the BCS theory [17], and further that the semi-empirical solution of the Eliashberg equations proposed by McMillan [38] could be applied to diamond, most theoretical studies have evaluated the critical temperature T_c through :

$$T_c = \hbar\omega_{log}/1.2k_B \exp[-(1.04(1+\lambda))/(\lambda-\mu^*(1+0.62\lambda))] \quad (1)$$

where ω_{log} is a logarithmic averaged phonon frequency (about 1020 cm^{-1} in diamond) and $\mu^* = g_F U_C(0)$ the strength of the zero frequency limit of the retarded Coulomb pseudopotential $U_C(0)$. This screening parameter, μ^*, has generally been taken by the authors to range between 0.1 [15], 0.13 [12] and 0.15 [13,14], either because these values lead to a good agreement with experiments or because the latter value is typical of usual metals where the Fermi energy is about two orders of magnitude greater than the phonon energy. Within a simplified parabolic band description of the valence band maximum and a BCS model for superconductivity, the curvature of the T_c vs n_B curve may then be discussed [4,5,29,39] as function of the λ and μ^* parameters governing equation (1).

Moreover, a comparison between (111)- and (100)-oriented p^{++} diamond epilayers [9,40] confirmed that above a threshold concentration n_c around 5 10^{20} cm^{-3}, T_c increased sub-linearly with n_B in the case of (100)-oriented growth and superlinear for (111)-oriented substrates. The fact that the same boron concentration could lead to quite different T_c values

depending on the preparation conditions [40] has raised the question of the doping efficiency of boron atoms depending on their incorporation site. For optimized growth conditions, the influence of such extrinsic mechanisms should however remain limited, in particular close to the critical boron concentration n_c [4,29]. As shown in fig 3.b, surprisingly large T_c values (> 0.4 K) have been obtained when n_B is only 10% higher than n_c in (100)-oriented epilayers where T_c followed a $(n_B/n_c-1)^{1/2}$ dependence.
Under the assumption that eq. (1) still applied despite the fact that close to n_c the Fermi energy becomes smaller than the phonon energy, those relatively high values of T_c could be explained [29] by a slow variation of the electron-phonon coupling parameter, λ, (typically $\lambda \sim (n_B/n_c-1)^{0.2}$), together with a pronounced but gradual decrease of the screening parameter μ^* when $n_B \rightarrow n_c$. Such a view, where both λ and μ^* are rescaled by the proximity of the Metal-to-Insulator Transition, is not so common, although the influence of the proximity of the MIT on the superconducting behaviour of disordered metals has been studied extensively over the last years in order to explain the enhancement of T_c in the vicinity of the MIT [41, 42]. Such an enhancement has not be reported for diamond so far.

Boron-doped diamond : a type II superconductor in the dirty limit

As indicated by the H_c vs T_c phase diagrams and $H_{c2}(0)$ values published in the first experimental studies [1,3,5], p^{++} diamond is a type II superconductor. A striking confirmation of this fact, featuring vortex images (see fig. 4a) obtained in the mixed state by ultra-low temperature STM [43], has been reported recently : the superconducting gap, its temperature dependence, its relationship to the macroscopic critical temperature, as well as the shape of the tunnelling density of states were found to be fully compatible with a conventional weak-coupling mechanism in a thin and homogeneous (100)-oriented epilayer. More precisely, in order to generate an image of the vortices, the scanning tip bias was fixed at the value corresponding to the coherence peak observed in the differential conductance spectra at the gap edge. A contrast on this signal was obtained when this peak disappeared in the locally normal regions present around each vortex core. These vortices formed a partially disordered triangular Abrikosov lattice (see fig. 4b) and were not pinned by defects or surface morphological features (fig. 4a). Spatial variations of the gap width as well as the temperature- and orientation-dependences of the gap shape [44] have however been observed, confirming the effect of spatial inhomogeneities on macroscopical signatures of superconductivity such as the marked broadening of the transition under moderate magnetic fields.
The coherence length, ξ, can be estimated either from the low T_c part of such phase diagrams or from the dH/dT slope at low field. Typical values for ξ evaluated in one of these ways were 10 nm for polycrystalline HPHT bulk p^{++} diamond [1], 10 to 30 nm for polycrystalline MPCVD films [4] and 15 and 20 nm for the (100)-oriented epilayers leading to the phase diagrams shown in fig. 4. An estimate of the mean free path, l_{mfp}, for the holes in the normal state has been proposed [4] on the basis of a combination of Hall effect and conductivity measurements at 4.2 K : l_{mfp} was on the order of 0.5 nm in samples where ξ = 10 nm. A London penetration length, λ_L, of 150 nm has moreover been evaluated for the same film. Seeing that $l_{mfp} << \xi << \lambda_L$, it was concluded that boron-doped superconducting diamond was in the dirty limit. Similar conclusions may be drawn from a free-electron description of the room temperature macroscopic conductivity values measured on superconductive films (usually in the 200-2000 $\Omega^{-1}cm^{-1}$ range), from momentum distribution curves of angle-resolved photoemission around the Fermi level (which yielded l_{mfp} = 0.5 and 0.9 nm in [44]), or from a Drude model analysis of their reflectivity spectrum (microscopic optical conductivity) yielding l_{mfp} = 2.5 and 4 nm at room temperature [35,45]. The latter values were obtained on the same epilayers mentioned above for which a phase diagram was published

and ξ values of 15 and 20 nm have been proposed [5] : again here, $l_{mfp} << \xi$. Moreover, in the thinnest of these boron-doped layers, both the room temperature scattering rate, γ, (from Drude analysis[45]) and the superconducting gap, $2\Delta(0)$, are known and there is no doubt that the $\gamma/2\Delta$ ratio is of the order of 1700, clearly in the "dirty" limit of superconductivity.

Conclusion

In p-type diamond, the critical boron doping of the metal-to-insulator transition (MIT) was found to coincide with that necessary for superconductivity to occur. Some of the critical exponents of the MIT were determined while superconducting diamond was found to follow a conventional type II behaviour in the dirty limit, with critical temperature values remaining relatively high quite close to the doping-induced insulator-to-metal transition. This could indicate that on the metallic side, both the electron-phonon coupling and the screening parameter depend on the boron concentration, in a range where the electronic energy of the system becomes smaller than the phonon energy.
Because diamond has a simple crystallographic structure and does not involve magnetism, it could become an attractive model-system for the study of superconductivity in low dimensional structures of controlled dimensions and where disorder can hopefully be restricted to the chemical randomness of an ideal substitutional alloy.

Acknowledgements

The authors are indebted to Dr C. Cytermann (Technion, Haifa) for SIMS profiling of the diamond epilayers, and to J. Kacmarcik (SAS, Kosice) for some of the low temperature transport measurements.

References

[1] E. A. Ekimov, V. A. Sidorov, E.D. Bauer, N.N. Mel'nik, N.J. Curro, J.D. Thompson and S.M. Stishov, Nature. **428**, 542 (2004).
[2] E. A. Ekimov, R. A. Sadykov, N.N. Mel'nik, A. Presz, E.V. Tat'yanin, V.N. Slesarev and N.N. Kuzin, Inorg. Mater. **40**, 932 (2004).
[3] Y. Takano, M. Nagao, I. Sakaguchi, M. Tachiki, T. Hatano,K. Kobayashi, H. Umezawa and H. Kawarada, Appl. Phys. Lett. **85**, 2851 (2004).
[4] K. Winzer, D. Bogdanov and Ch. Wild, Physica C **432**, 65 (2005).
[5] E. Bustarret, J. Kačmarčik, C. Marcenat, E. Gheeraert, C. Cytermann, J. Marcus and T. Klein, Phys. Rev. Lett. **93**, 237005 (2004).
[6] V.A. Sidorov, E.A. Ekimov, E.D. Bauer, N.N. Mel'nik, N.J. Curro, V. Fritsch, J.D. Thompson, S.M. Stishov, A.E. Alexenko and B. Spitsyn, Diam. Rel. Mater. **14**, 335 (2005).
[7] Z.L. Wang, Q. Luo, L.W. Liu, C.Y. Li, H.X. Yang, H.F. Yang, J.J. Li, X.Y. Lu, Z.S. Jin, L. Lu and C.Z. Gu., Diam. Rel. Mater. **15**, 659 (2006).
[8] M. Nesladek, D. Tromson, C. Mer, P. Bergonzo, P. Hubik and J.J. Mares, Appl. Phys. Lett. **88**, 232111 (2006).
[9] H. Mukuda, T. Tsuchida, A. Harada, Y. Kitaoka, T. Takenouchi, Y. Takano, M. Nagao, I. Sakaguchi, T. Oguchi and H. Kawarada, Phys. Rev. B75, 033301 (2007).
[10] J. Nagamatsu, N. Nakagawa, T. Muranaka, Y. Zenitani and J. Akimitsu, Nature **410**, 63 (2001).
[11] N. Emery, C. Hérold, M. d'Astuto, V. Garcia, Ch. Bellin, J.F. Marêché, P. Lagrange and G. Loupias, Phys. Rev. Lett. **95**, 087003 (2005).
[12] X. Blase, Ch. Adessi and D. Connétable, Phys. Rev. Lett. **93**, 237004 (2004).
[13] H.J. Xiang, Z. Li, J. Yang, J.G. Hou and Q. Zhu, Phys. Rev. **B70**, 212504 (2004).
[14] K.-W. Lee and W.E. Pickett, Phys. Rev. Lett. **93**, 237003 (2004).
[15] L. Boeri, J. Kortus and O.K. Andersen, Phys. Rev. Lett. **93**, 237002 (2004).
[16] Y. Ma, J.S. Tse, T. Cui, D.D. Klug, L. Zhang, Yu Xie, Y. Niu and G . Zou, Phys. Rev. **B72**, 014306 (2005).
[17] J. Bardeen, L.N. Cooper and J.R. Schrieffer, Phys. Rev. **108**, 1175 (1957).
[18] D. Pines, Phys. Rev. **109**, 280 (1958).
[19] M.L. Cohen, Phys. Rev. **134**, A511 (1964) ; M.L. Cohen, Rev. Mod. Phys. **37**, 240 (1964) ; M.L. Cohen, in *Superconductivity* (R.D. Parks ed.) vol. 1, Marcel Decker, New York, 1964, p. 615.
[20] P.J. Stiles, L. Esaki and J.F. Schooley, Phys. Lett. **23**, 206 (1966).
[21] E. Bustarret, C. Marcenat, P. Achatz, J. Kačmarčik, F. Lévy, A. Huxley, L. Ortéga, E. Bourgeois, X. Blase, D. Débarre and J. Boulmer, Nature **444**, 465 (2006).
[22] F. Brunet, P. Germi, M. Pernet, A. Deneuville, E. Gheeraert, F. Laugier, M. Burdin and G. Rolland, J. Appl. Phys. **83**, 181 (1998).

[23] E. Bustarret, E. Gheeraert and K. Watanabe, phys. stat. sol. (a) **199**, 9 (2003).
[24] V.V. Brazhkin, E. A. Ekimov, A.G. Lyapin, S.V. Popova, A.V. Rakhmanina, S.M. Stishov, V.M. Lebedev, Y. Katayama and K. Kato, Phys. Rev. **B74**, 140502 (R) (2006).
[25] E. Bourgeois, E. Bustarret, P. Achatz, F. Omnès and X. Blase, Phys. Rev. **B74**, 094509 (2006).
[26] J. Kačmarčik, C. Marcenat, C. Cytermann, A. Ferreira da Silva, L. Ortéga, F. Gustafsson, J. Marcus, T. Klein, E. Gheeraert and E. Bustarret, phys. stat. sol. (a) **202**, 2160 (2005).
[27] Y. Kato, F. Matsui, T. Shimizu, T. Matsushita, F.Z. Guo, T. Tsuno and H. Daimon, Sci. Technol. Adv. Mater. **7**, S45 (2006).
[28] C. Uzan-Saguy, A. Reznik, C. Cytermann, R. Brener, R. Kalish, E. Bustarret, M. Bernard, A. Deneuville, E. Gheeraert and J. Chevallier, Diam. Rel. Mater. **10**, 453 (2001) ; J.P. Goss, P.R. Briddon, R. Jones, Z. Teukam, D. Ballutaud, F. Jomard, J. Chevallier, M. Bernard and A. Deneuville, Phys. Rev. **B68**, 235209 (2003).
[29] T. Klein, P. Achatz, J. Kačmarčik, C. Marcenat, F. Gustafsson, J. Marcus, E. Bustarret, J. Pernot, F. Omnès, Bo E. Sernelius, C. Persson, A. Ferreira da Silva and C. Cytermann, Phys. Rev. **B75**, 165313 (2007).
[30] Y. Takano, M. Nagao, T. Takenouchi, H. Umezawa, I. Sakaguchi, M. Tachiki and H. Kawarada, Diam. Rel. Mater. **14**, 1936 (2005).
[31] T. Tshepe, J.F. Prins and M.J.R. Hoch, Diam. Rel. Mater. **8**, 1508 (1999).
[32] N.F. Mott, J. Non Cryst. Sol. **1**, 1 (1968).
[33] A.L. Efros and B.I. Shklovskii, J. Phys. C Sol. St. Phys., **8**, L49 (1975) ; A.L. Efros ,J. Phys. C Sol. St. Phys. **9**, 2021 (1976).
[34] T. Sato, K. Ohashi, H. Sugai, T. Sumi, K. Haruna, H. Maeta, N. Matsumoto and H. Otsuka, Phys. Rev. **B61**, 12970 (2000).
[35] J.J. Mares, P. Hubik, M. Nesladek, D. Kindl and J. Krištofik, Diam. Rel. Mater. **15**, 1863 (2006).
[36] W.L. McMillan, Phys. Rev. **B24**, 2739 (1981) and references therein.
[37] A.S. Barnard, S.P. Russo and I.K. Snook, Phil. Mag. **83**, 1163 (2003).
[38] W. L. McMillan, Phys. Rev. **167**, 331 (1968).
[39] M. Cardona, Sol. St. Comm. **133**, 3 (2005) ; Sci. Technol. Adv. Mater. **7**, S60 (2006).
[40] H. Umezawa, T. Takenouchi, Y. Takano, K. Kobayashi, M. Nagao, I. Sakaguchi, A. Ishii, M. Tachiki, T. Hatano, Guofang Zhong, M. Tachiki and H. Kawarada, cond-mat/0503303.
[41] M.S. Osofsky, R.J. Soulen, Jr., J.H. Claassen, G. Trotter, H. Kim and J.S. Horwitz, Phys. Rev. Lett. **87**, 197004 (2001) ; *ibid*, Phys. Rev. **B66**, 020502 (R), (2002).
[42] R. J. Soulen, M.S. Osofsky and L.D. Cooley, Phys. Rev. **B68**, 094505 (2003).
[43] B. Sacépé, C. Chapelier, C. Marcenat, J. Kacmarcik, T. Klein, M. Bernard and E. Bustarret, Phys. Rev. Lett. **96**, 097006 (2006) ; B. Sacépé, C. Chapelier, C. Marcenat, J. Kačmarčik, T. Klein, F. Omnès and E. Bustarret, phys. stat.sol. (a) **203**, 3315 (2006).
[44] T. Yokoya, T. Nakamura, T. Matsushita, T. Muro, Y. Takano, M. Nagao, T. Takenouchi, H. Kawarada, T. Oguchi, Nature **438**, 647 (2005).
[45] E. Bustarret, F. Pruvost, M. Bernard, C. Cytermann and C. Uzan-Saguy, phys. stat. sol. (a) **186**, 303 (2001).

Figure legends

Figure 1a
Iso-intensity contours around the {400} diffraction peak of a (100)-oriented heavily B-doped diamond epilayer. The abscissa axis corresponds to the 2 theta minus omega ($2\theta - \omega$) scanning direction while the vertical axis corresponds to the omega (ω) offset angle (rocking curve).

Figure 1b
Iso-intensity contours around the {111} diffraction peak of a miscut (111)-oriented heavily B-doped diamond epilayer. The abscissa axis corresponds to the 2 theta minus omega ($2\theta - \omega$) scanning direction while the vertical axis corresponds to the omega (ω) offset angle (rocking curve).

Figure 2
Temperature dependence of the a.c. resistivity (four point) of various (100)-oriented diamond epilayers with different boron contents n_B measured by SIMS. The doping-induced MIT is found to occur between 4.0 and 4.8 10^{20} cm^{-3}.

Figure 3a
Conductivity extrapolated to zero temperature as a function of the boron content, n_B, deduced from SIMS measurements on boron-doped diamond (100)-oriented epilayers. The solid line corresponds to the prediction of the scaling theory of the Metal-to-Insulator transition, taking $\nu = 1$ (see text). Insert : Temperature dependence of the electrical resistance (for two samples also characterised in fig. 2), rescaled to their resistance at 100 K, illustrating the weak localization regime (more pronounced closer to the MIT) and the definition of T_c for the superconducting transition.

Figure 3b
Critical temperature T_c deduced from resistivity curves (at 90% of the normal state resistance) as a function of the boron content n_B deduced from SIMS measurements. The open circle has been taken from ref. 1. The solid line corresponds to $T_c \sim (n_B/n_c-1)^{0.5}$ with $n_c = 4.5\ 10^{20}$ cm^{-3}.

Figure 4a
Vortex image (1.5 x 1.5 μm^2) obtained at 100 mK at a magnetic field of 1900 Oe on a (100)-oriented 75 nm-thick boron-doped diamond epilayer, superimposed with a topographic STM map yielding an rms roughness of 1.8 nm. The vortices appear as darker spots.

Figure 4b
Fourier transform mapping of the vortex image shown in fig. 4a, illustrating the disorder affecting the triangular Abrikosov lattice. The average vortex spacing was 110 nm.

Fig.1a

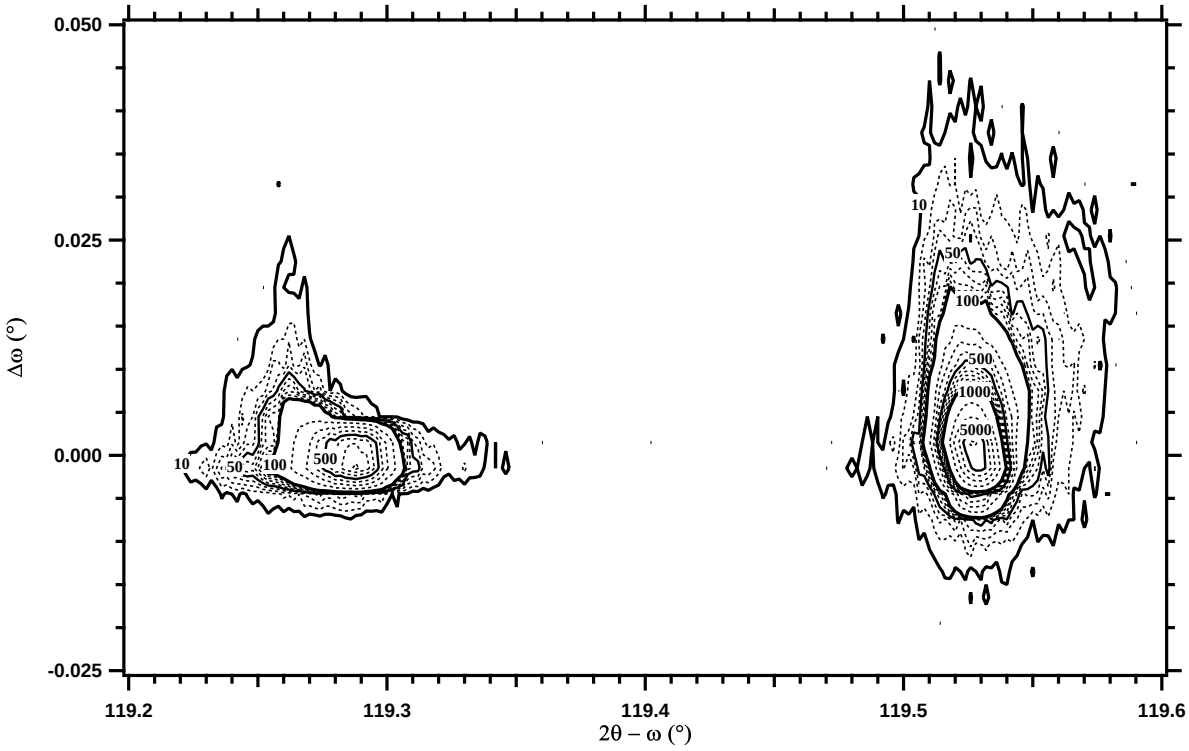
0.050
0.025
0.000
-0.025
Δω (°)
119.2
119.3
119.4
119.5
119.6
2θ – ω (°)
10
50
100
500
10
50
100
500
1000
5000

Fig.1b

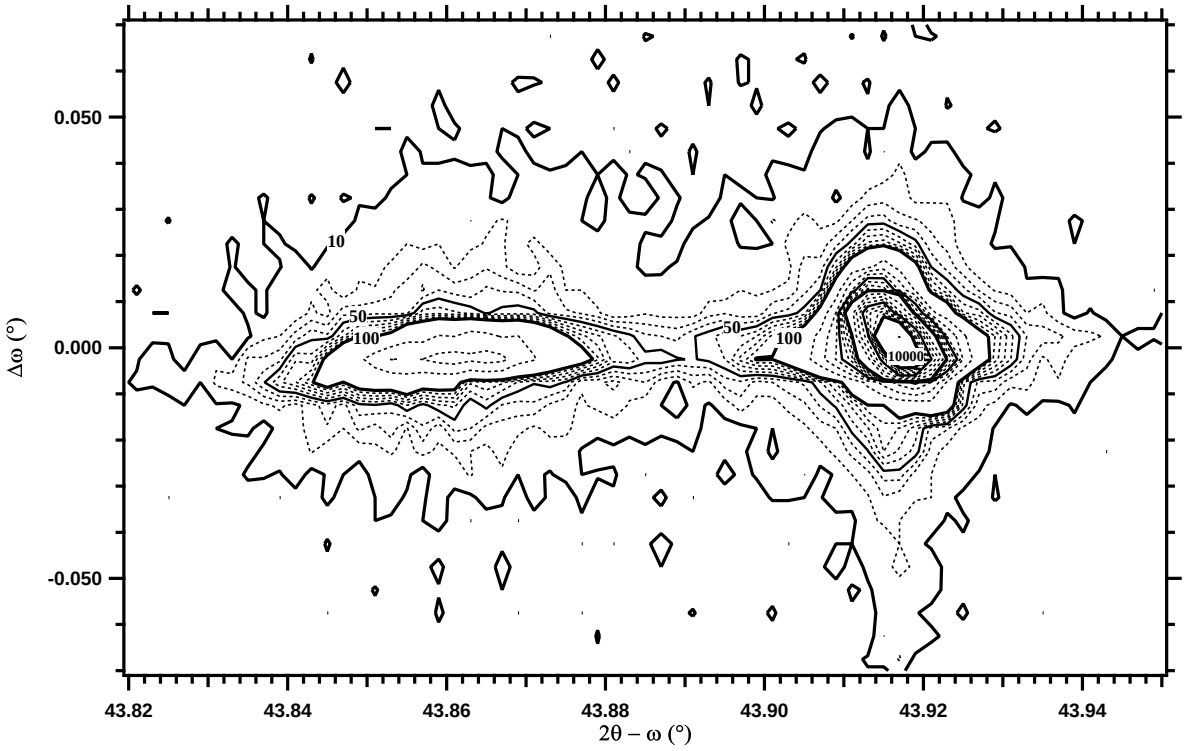
0.050
0.000
-0.050
Δω (°)
10
50
100
50
100
10000
43.82
43.84
43.86
43.88
43.90
43.92
43.94
2θ – ω (°)

Fig.2

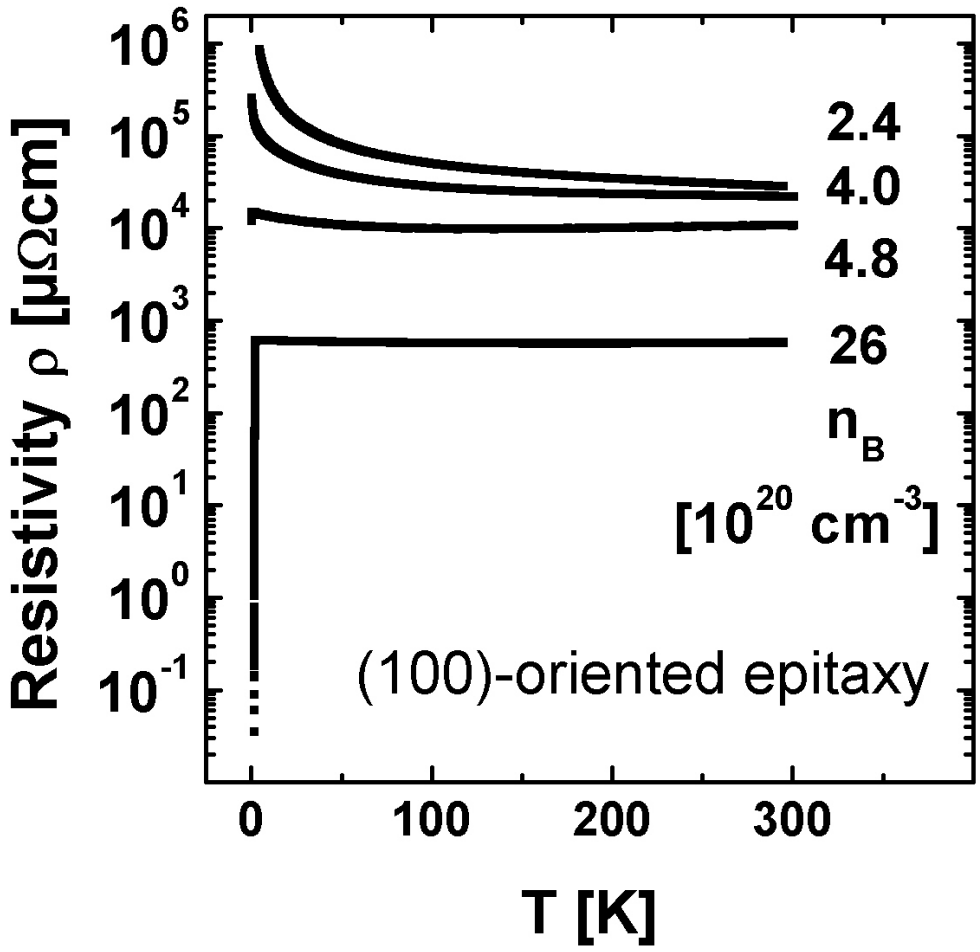
Resistivity ρ [μΩcm]
10^6
10^5
10^4
10^3
10^2
10^1
10^0
10^-1
2.4
4.0
4.8
26
n_B
[10^20 cm^-3]
(100)-oriented epitaxy
0
100
200
300
T [K]

Fig.3a & b

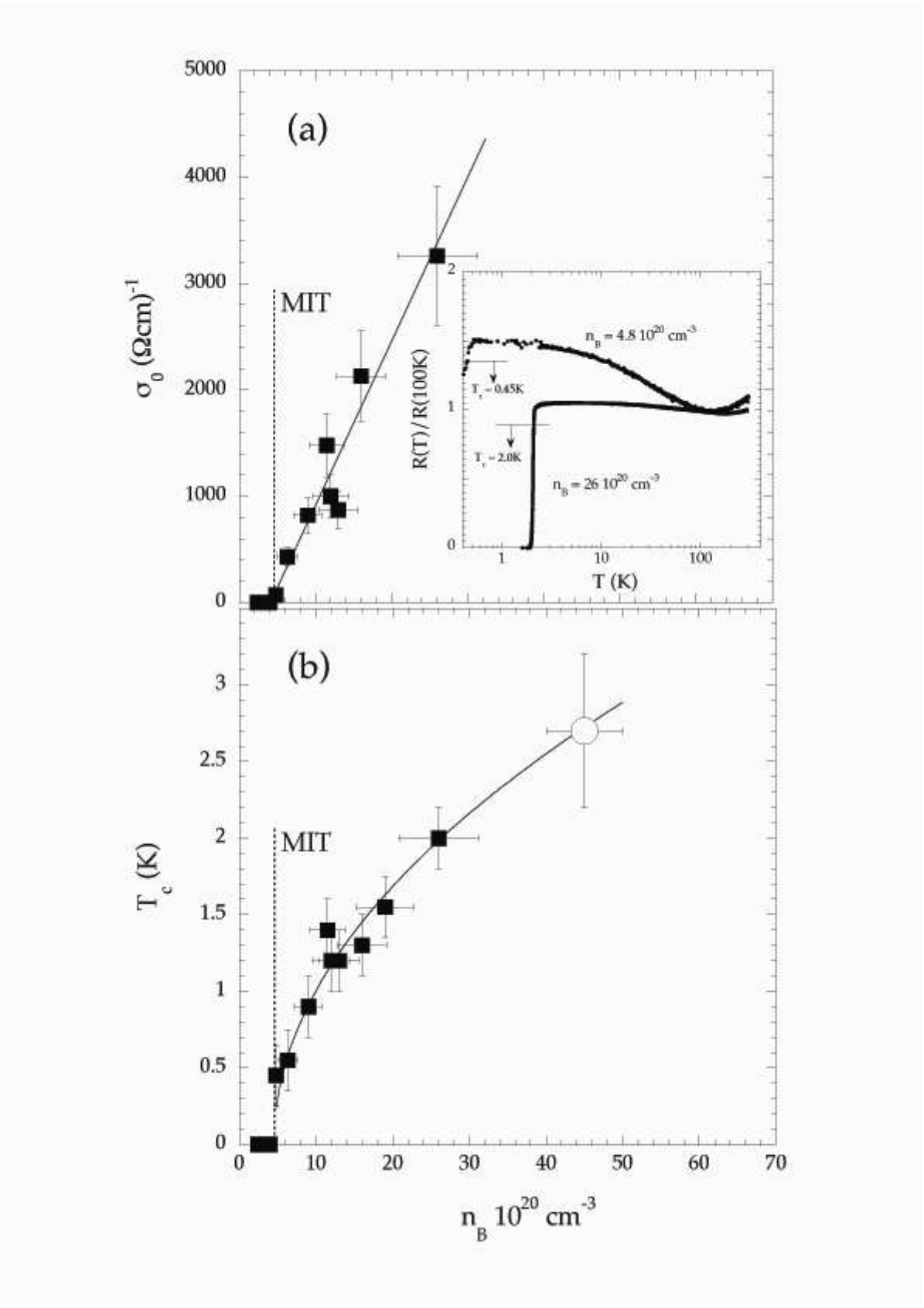
(a)
MIT
σ_0 $(\Omega cm)^{-1}$
5000
4000
3000
2000
1000
0
R(T)/R(100K)
2
1
0
$n_B = 4.8\ 10^{20}\ cm^{-3}$
$T_c = 0.45K$
$T_c = 2.0K$
$n_B = 26\ 10^{20}\ cm^{-3}$
1
10
100
T (K)
(b)
MIT
T_c (K)
3
2.5
2
1.5
1
0.5
0
0
10
20
30
40
50
60
70
$n_B\ 10^{20}\ cm^{-3}$

Fig. 4a

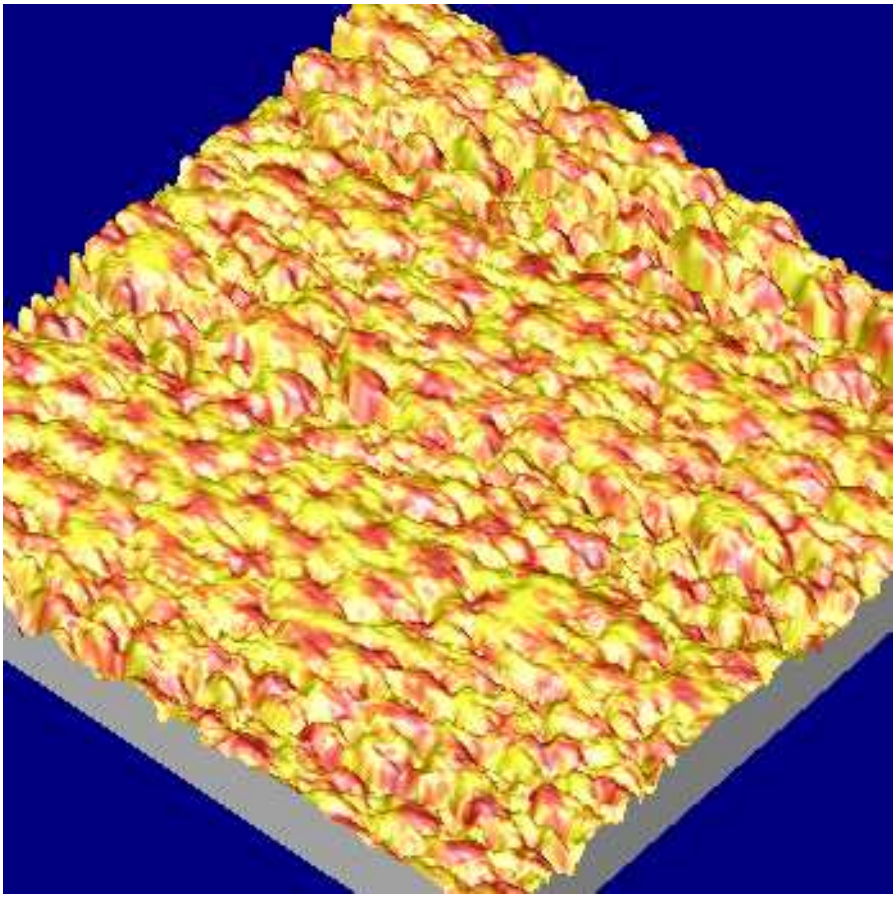

Fig. 4b